Planar radiative shock experiments and their comparison to simulations[a)]

A. B. Reighard,[1,b)] R. P. Drake,[1] J. E. Mucino,[1] J. P. Knauer,[2] and M. Busquet[3]
[1]*Department of Atmospheric Oceanic and Space Sciences, University of Michigan, Ann Arbor, Michigan 48109*
[2]*Laboratory for Laser Energetics, University of Rochester, Rochester, New York 14627*
[3]*Observatoire de Paris, 5 place J. Janssen, 92195 Meudon, France*

(Received 3 November 2006; accepted 14 February 2007; published online 26 April 2007)

Recent experiments have obtained radiographic data from shock waves driven at >100 km/s in xenon gas, and Thomson scattering data from similar experiments using argon gas. Presented here is a review of these experiments, followed by an outline of the discrepancies between the data and the results of one-dimensional simulations. Simulations using procedures that work well for similar but nonradiative experiments show inconsistencies between the measured position of the interface of the beryllium and xenon and the calculated position for these experiments. Sources of the discrepancy are explored. © *2007 American Institute of Physics*. [DOI: 10.1063/1.2714023]

I. INTRODUCTION

Radiation hydrodynamics is a difficult regime to explore in laboratory systems. It requires facilities capable of heating moderate-density material to relatively high temperatures in a system of large enough extent to allow the radiation transport to affect the hydrodynamic properties of the system. Here, after discussing prior related work and some of the astrophysical connections of our work, we describe an experiment producing a radiation hydrodynamic, driven shock in xenon gas and one-dimensional (1D) simulations of that experiment. A notable discrepancy is present in the predicted driver/gas interface versus the measured experimental position of the interface. We proceed to explore some possible causes of the discrepancy.

The present experiments are the first in planar geometry to exceed the threshold for radiative collapse by formation of a post-shock cooling layer, and to detect the material that has been shocked and cooled. Following the shock, which heats ions primarily, the ions and electrons equilibrate rapidly. A post-shock cooling layer must form when the energy flux due to thermal radiative losses from the shocked material exceeds the energy flux entering the shocked material. The natural normalization of the fluid energy equation in an optically thick system gives a threshold for significant radiative cooling as $R_r > 1$, where

$$R_r = \frac{(\gamma+1)}{\gamma}\frac{4\sigma T_{\mathrm{init}}^4}{\rho_o u_s^3} \propto \frac{u_s^5}{\rho_o}, \tag{1}$$

in which σ is the Stefan-Boltzmann constant and ρ_o is the mass density of the unshocked, upstream material. The corresponding threshold velocity in xenon, at 10 mg/cm^3, is about 50 km/s.[1] If the optical depth of the region behind the shock decreases, decreasing the emissivity of the shocked material, the value of R_r required to see large radiative effects increases.

Prior work has included a number of experiments that have exceeded the shock-velocity threshold[2] for the formation of a thermal radiative precursor, in which thermal radiation from matter heated by the shock itself heats the matter ahead of ("upstream" of) the shock. Radiative precursors have been observed in experiments by Bozier *et al.*,[3] Grun *et al.*,[4] Keiter *et al.*,[2] González, Busquet, and co-workers,[5,6] and Koenig, Bouquet, and co-workers.[7–11] The experiments of Grun *et al.*[12] and Hansen *et al.*[13] produced quasispherical radiative blast waves at much lower density, with significant radiative effects. Experiments producing a cylindrical blast wave observed radiative cooling effects caused by heating of the shocked gas by electron heat conduction.[14]

The experiments discussed here were motivated by the need to better understand radiative shocks in astrophysics. Astrophysical radiative shocks appear in a wide range of contexts. Depending on the details of the strength of the shock and the circumstellar material, shocks in young supernova remnants may be radiative.[15] Some astrophysical jets show signs of radiative cooling and compression.[16] Some stationary shocks in stellar atmospheres can radiatively cool efficiently.[17] Aging supernova remnants pass into a radiative phase when the radiative cooling time becomes shorter than the age of the remnant.[18]

Because the properties of such shocks depend fundamentally on the optical depth of the upstream and downstream regions,[19] any specific experiment is most relevant to astrophysical cases with a similar structure of optical depth. Figure 1 shows one example of this for the present experiment. In simulations of shock breakout in SN1987a by Ensman and Burrows (1992),[20] the authors note the formation of a radiative cooling layer just behind the shock driven by the stellar explosion as it enters the lower-density material in the outer layers of the star. Rapid radiative cooling of the shocked material was accompanied by a sharp density increase, as shown in Fig. 1(a). The thickness of this dense layer is very small compared to the distance from the center of the star. This is similar to the formation of a cooling layer in an experiment driving a shock through xenon gas, described in the present paper and further[21] by Reighard *et al.*

[a)]Paper NI2 6, Bull. Am. Phys. Soc. **51**, 180 (2006).
[b)]Invited speaker.

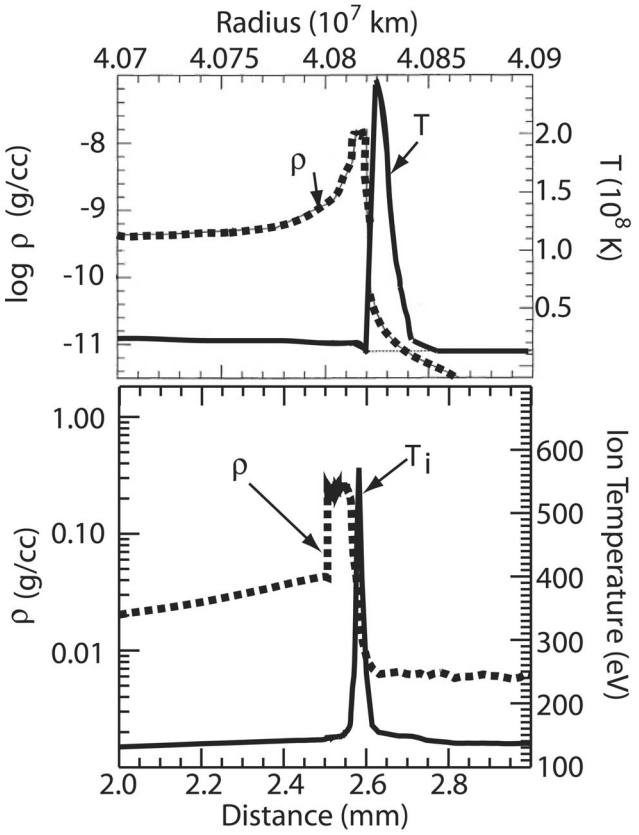

FIG. 1. Profiles of density (dashed) and ion temperature (solid) in two radiative shocks that are optically thick downstream and optically thin upstream. (a) Temperature and density profiles obtained by Ensman and Burrows, modeling the shock in SN 1987A as it emerges from the star. From Ensman and Burrows, 1992. (b) Temperature and density profiles from simulations of the present experiments in xenon gas.

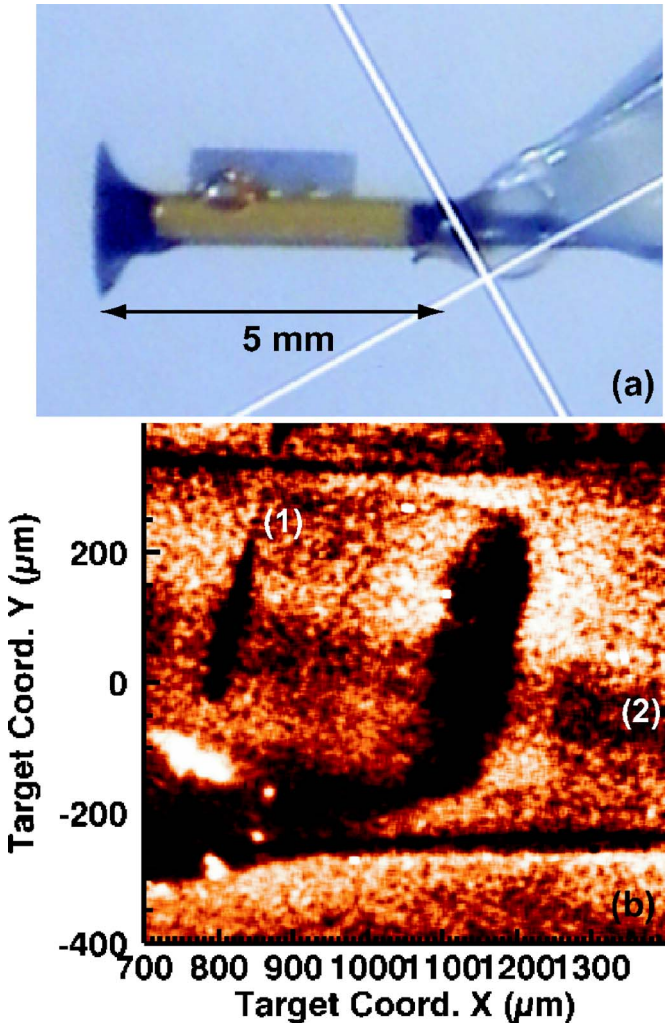

FIG. 2. (Color online) (a) An image of the radiative shock target. The 20 μm thick beryllium disk (left) is accelerated via laser ablation pressure into a xenon-filled polyimide tube. The tube diameter is 600 μm. The object attached to the top of the tube is a gold grid used for spatial calibration. A tube used for filling the target with gas before experiments is shown on the right of the tube. (b) X-ray radiography image of collapsed radiative shock at 8 ns after the drive lasers turn on. Position is measured from the front side of the initial position of the beryllium disk. The dark feature is dense xenon gas, while the beryllium is transparent at this wavelength. Two of the observed features do not represent real structure. The dark feature labeled "1" to the left of the Be/Xe interface is due to a scratch on the film. The nearly horizontal, moderately dark feature across the entire image, labeled "2," is noise produced by the framing camera when operated at this pulse length.

A simulation showing the density and temperature structure behind the shock for the experiment is shown in Fig. 1(b). In both of these systems, the material downstream of the shock is optically thick and moving at a high velocity, which shocks lower-density material to a high temperature. This hot, shocked gas then radiates strongly and loses significant amounts of energy, causing further compression of the shocked material. It is important to note that while the present experiment can observe the qualitative structural evolution of this type of system, and can be directly useful for validation of simulation codes, it is not a completely well-scaled model of the astrophysical case. The reason is that the scaling of the radiative cooling and heating with density and temperature in the two systems is not identical.[19] Even so, any computer code intended to accurately simulate shocks in astrophysics with this structure should also be able to simulate the shock in the present experiment.

II. EXPERIMENT DESCRIPTION AND RESULTS

The experiments were performed at the Omega laser at the Laboratory for Laser Energetics at the University of Rochester.[22] Figure 2(a) shows an image of one of the targets used. The gas cell was a cylindrical section of polyimide tubing, of inside diameter (ID) 600 μm and composition $C_{22}H_{10}N_2O_5$. We used the metallic tube attached to the right end of the target to evacuate it and then fill it with xenon. The xenon pressure was measured immediately before the laser firing for each experiment. It was 1.1 (±10%) ATM for the cases of interest here corresponding to ρ_o=0.006 g/cm^3 or to 2.7×10^{19} atoms/cm^3. Shown attached to the left end of the target, a circular metallic disk, identified here as the "drive disk," is attached to the polyimide tube using glue. For the experiments discussed here, the drive disk was beryllium, 20 μm (±7%) thick and 2 mm in diameter. We focused ten laser beams of wavelength 0.35 μm onto a ~1 mm spot centered on the drive disk. The laser beam pulse was square, with a 1-ns flat-top pulse, and with the midpoint of the rising edge defining time t=0. The total energy was≤4000 J. Distributed Phase Plates (DPPs) created

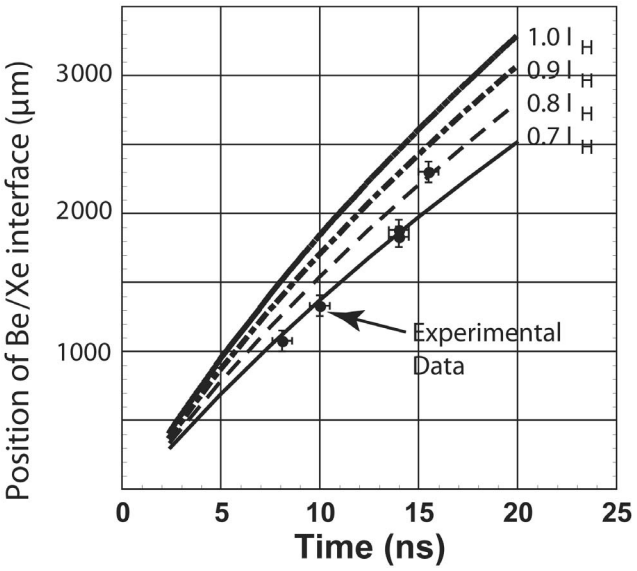

FIG. 3. Measured position of the beryllium/xenon interface, as well as predicted interface positions from simulations at reduced fractions of the nominal drive laser irradiance, I_H, as indicated. At full nominal laser irradiance, the simulations overpredict the interface position by 25%.

super-Gaussian focal spots of 820 μm diameter [full width at half-maximum (FWHM)], with small-scale structure that fluctuated via Smoothing by Spectral Dispersion (SSD).[23] The overlapping laser beams produced a laser irradiance of approximately 5×10^{14} W/cm^2. The pressure from laser ablation drives a shock through the drive disk and then continues to accelerate the resulting Be plasma, propelling it into the tube, where the Be drives a shock into the xenon.

We diagnosed these experiments using three diagnostics. The primary diagnostic was x-ray radiography, typically using a backlit pinhole to produce a cone of 5.2 keV He-α-like x rays, created by focusing four laser beams on a 5-μm-thick vanadium foil, located behind a 20 μm pinhole in a Ta substrate. This cone of x rays irradiated the target and was recorded by a gated, microchannel-plate framing camera of a standard type.[24] Figure 2(b) shows a radiographic image from such an experiment. This image, viewing along a line of sight orthogonal to the tube axis, was captured at 8 ns after the drive beams fired. The dark absorption feature is the dense xenon gas, which is moving to the right in this image. The shock front is at the right edge of the observed dark feature and the beryllium/xenon interface is at the left edge. In these radiographic images, the beryllium driver is transparent, so no features of the beryllium are measured by this diagnostic. The xenon layer is not orthogonal to the tube axis, which we attribute to errors in the alignment of the target to the beams. Figure 3 shows the position of the interface obtained from a sequence of experiments, along with some curves from simulations to be discussed. The error bars on these data points are from uncertainty in drive timing in time and from uncertainty in metrology measurements in position. Further details and results of the experiment and the radiographic data can be found in Reighard *et al.*[21] The second diagnostic used was Thomson scattering from shocks driven in argon gas[25] and we used transverse velocity interferometry,[26] (VISAR[27]) in xenon to obtain further evidence of the behavior of these shocks as a third diagnostic.

These measurements led consistently to the following description of the behavior of these shocks. The radiography shows that Be plasma pushes the Xe forward at a velocity of 135 ± 10 km/s, approximately constant (ignoring one outlying point) from 8 to 15 ns. It also shows that the xenon is compressed to a thin layer. Obtaining the exact compression is complicated by tilting of the shocked layer and other effects, but notwithstanding these limitations it is clear that the xenon layer has collapsed in space during radiative cooling. The collapse occurs because the pressure in the xenon is sustained by the Be and newly shocked Xe even as the shocked xenon is compressed to several times its initial post-shock density.[21] The Xe radiates strongly because the post-shock electron temperature reaches several hundred eV. (The simulations discussed below give 230 eV, while one finds 250 eV from a simple model based on the shock velocity and Saha ionization.[19] In addition, after allowing for the differences between Xe and Ar, the Thomson scattering measurements made in argon gas are reasonably consistent with these numbers.) In experiments using a 40 μm drive disk, the VISAR measurement showed that the precursor has become ionized, and confirmed the shock velocity determined by the radiography.[26]

III. BASIC SIMULATIONS AND RESULTS

Our one-dimensional simulations of this system used Hyades,[28] a Lagrangian code using a single continuity equation and single momentum equation, separate energy equations for the electrons and the ions, and, in the simulations discussed here, treating radiation with flux-limited multigroup diffusion. The average ionization is taken to have its equilibrium value and opacities are evaluated using an average atom model. The equation of state is either tabular or that of a polytropic gas with a specified index, γ. Electron heat transport is by flux-limited diffusion. In some cases, radiation is artificially suppressed.

We simulate the launching of a beryllium disk into xenon gas at 1.1 ATM, or 0.006 g/cm^3. The beryllium is finely zoned, using 165 zones over 20 μm of material. These zones are feathered to smaller sizes in the zones closest to the xenon. The equation of state used for beryllium was an ideal gas model using $\gamma=1.6$. The resulting behavior was identical to that seen in other cases using a SESAME equation of state table,[29] which is not surprising as the ~50 Mbar shock driven by the laser fully ionizes the Be. The xenon gas was modeled using a total of 400 zones over 4 mm, with smaller zones closer to the beryllium interface, and used a SESAME equation of state. The radiation was treated with 90 photon groups over 20 keV, adjusted to resolve edges in xenon up to 6 keV. The left edge of the beryllium in these simulations was irradiated using a laser source at 3.4×10^{14} W/cm^2 for 1 ns, which is 66% that used in the experiment. We will refer to this quantity in the discussion below as I_H.

As has been observed through 2D simulations,[30] the laser irradiance used in 1D simulations at the irradiance of interest here must be reduced to give accurate results, be-

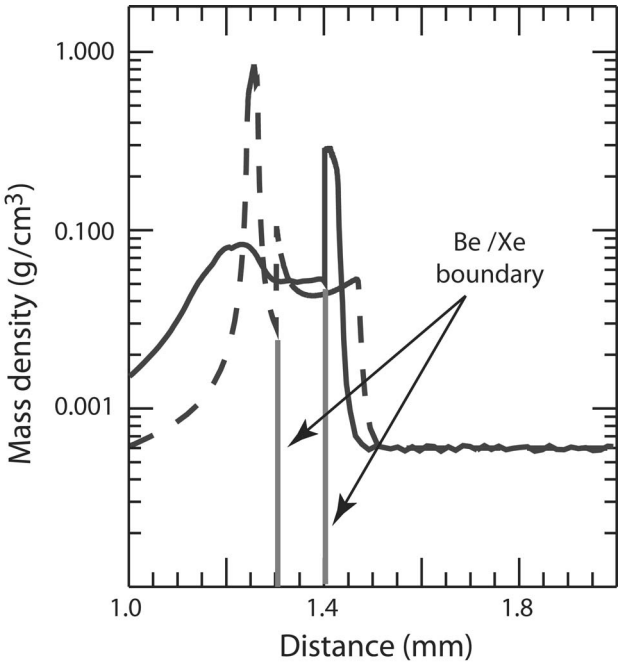

FIG. 4. Density profiles from Hyades simulations of the experiment at 8 ns. The solid line is a simulation using diffusive multigroup radiation transport, while the dashed line is an identical simulation with radiation artificially suppressed. The vertical line extending from both curves to the *x* axis shows the location of the beryllium/xenon interface for each simulation.

cause radial heat transport reduces the ablation pressure in the actual system. The irradiation in the present experiments is nearly identical to that used in previous work with two-layer, nonradiative, purely hydrodynamic targets,[31] differing only in these ways: (a) the present experiments use SSD, (b) the present experiments use an irradiance that is 80% of the value used previously, and (c) the present experiments use 20 μm of Be, from which the shock emerges during the laser pulse, while the previous experiments used 150 μm of polyimide as a first layer, so that the shock traversed only about half of this layer during the laser pulse. In the previous work, we have extensively compared the results of Hyades simulations to measurements of the shock and interface positions. We found that the code reproduced the observations very well using an irradiance that was 66% of the actual value. Here, we used as I_H 66% of the laser irradiance in the present experiments. Given the similarity of the irradiation conditions, it seems sensible to assume that the lateral energy transport during laser irradiation ought to be the same in the present experiment, and so one expects that simulations using an irradiation of I_H ought to match the data.

These simulations predict the production of a dense, collapsed layer in the shocked xenon gas. After an initial formation period, a quasi-steady-state shocked layer forms, showing a compressed layer of xenon that is approximately 50 times more dense than the unshocked xenon gas. At 8 ns, as shown in the solid line in Fig. 4, the collapsed layer is approximately 65 μm thick after having traveled 1.4 mm. In this figure, the vertical line indicates the position of the boundary between beryllium and xenon. These simulations also show a lower-density region of beryllium separating the xenon layer from the bulk of the beryllium pusher. We attribute this to the radiation from the xenon, which ablates the leading edge of the Be.[32] For comparison, identical simulations were done with radiation transport artificially suppressed, with results shown by the dashed line in Fig. 4. In these simulations, the shocked material in xenon gas formed an extended layer that was 200 μm thick and only 10 times as dense as the unshocked xenon gas. There is little separation between the xenon and the beryllium, and the bulk of the beryllium remains very dense. One can see that the beryllium density at the interface with the xenon is much higher in the radiative simulation, and that the interface has moved 100 μm farther than in the simulation where radiation was suppressed.

TABLE I. Parameters from a simulation matching the data.

	Location (μm)	T_e (eV)	T_i (eV)	T_r (eV)	Z
Interface	1360	47	47	41	11.2
Equilibration point	1397	66	66	46	14.6
Temperature peak	1405	81	335	44	18.3

Contrary to the expectations discussed above, simulations run with laser irradiance I_H did not reproduce the observations. There is a significant discrepancy between the observed and simulated positions of the beryllium/xenon interface, as Fig. 3 shows. The uppermost curve in Fig. 3 is a 1D Hyades simulation run at the irradiance I_H described above. This curve lies well above the experimental data, overpredicting the distance the interface has traveled by approximately 25%. The other curves on the plot show the effect on the interface position of decreasing the laser irradiance. To obtain the observed trajectory of interface locations, the laser irradiance must be reduced to 0.7 I_H (29% of the actual laser irradiance). While this represents a method of reproducing the observed interface position using the code, it is an *ad hoc* adjustment for which we do not have a physical basis. This motivates the discussion of the following section.

Table I shows, at 10.0 ns, several parameters of this system from the simulation that reproduces the observed interface position. The table gives values at the interface location, at the zone where the electron temperature T_e and ion temperature T_i equilibrate to within 1 eV, and at the zone of maximum T_i. It gives the location, T_e, T_i, the average charge, Z, and the radiation "temperature" T_r, which is the value of the temperature that corresponds for a Planckian distribution to the radiation energy density. At the equilibration point, the electron density is 7.1×10^{21} cm^{-3}. Although the radiation flux is clearly important to the dynamics of this system, the radiation pressure remains nearly four orders of magnitude smaller than the plasma pressure.

IV. EXPLORING DISCREPANCIES BETWEEN 1D SIMULATIONS AND EXPERIMENTAL RESULTS

This section reports the results of our examination of the possible causes of the discrepancy just described. It might be a consequence of either the one-dimensional dynamics of the system or of two-dimensional effects. The potential physical

issues that could create errors in the one-dimensional location of the Be/Xe interface include the equation of state of the Be, the effect of radiation in the Be as it is shocked and accelerated, and the effect of the radiation from the Xe on the Be as the shock evolves. Here we first consider possible two-dimensional effects and then consider the issues in one dimension just mentioned.

In two-dimensional simulations, one may find the lateral flow of energy or matter, which cannot be accounted for in a one-dimensional simulation. The lateral flow of energy during the laser pulse acts to reduce the ablation pressure and thus may reduce the momentum delivered to the Be plasma. The use of the irradiance I_H in our baseline simulations is intended to account for this. We would not expect the lateral flow of energy after the laser pulse to have a significant effect on the Be/Xe interface position, which must be determined primarily by momentum balance. The momentum of the Be plasma has already been established during the laser pulse, and the initial areal mass of the Be drive disk is equivalent to 6 mm of the Be gas. In addition, lateral flow of energy is present in simulations of similar experiments using the FCI code, reported previously.[21] FCI includes laser absorption, radiation, and flux-limited diffusive electron heat transport. The FCI simulations exhibited a discrepancy similar to that seen in the 1D results presented above. The lateral flow of matter could potentially have an impact on the Be/Xe interface location through its effect on the momentum balance or on the thickness of the Be plasma. However, simulations with FCI and with Zeus[33,34] did not produce significant lateral mass flow. We had only a limited ability to learn from two-dimensional simulations, but the considerations just stated made it seem plausible that the cause of the discrepancy might be one of the one-dimensional effects identified in the previous paragraph. This motivated a more extensive exploration of the one-dimensional issues, described here.

Because the shock velocity and collapsed layer position in these experiments and simulations depend on the position of the driven surface, we first undertook to examine the treatment of the beryllium in the simulations more closely. We first explored the possibility that errors in the Be equation of state (EOS) might be important and then explored the impact of the treatment of radiation on the Be evolution. We explored the sensitivity to EOS by doing a sequence of simulations varying γ. While this might fail to capture details associated with changes in compressibility as different electron shells open up in the material, it should show whether the behavior of the system is strongly sensitive to the EOS. In addition, for Be shocked to 50 Mbars it would be quite surprising to find subtle differences relating to the detailed structure of the equation of state. We found that variations in γ produced the expected increase or decrease of the Be density but led to only small changes in the interface velocity. This is not surprising as the ablation pressure and mass ablation rate due to the laser should be weakly affected by changes in compressibility, so that the main determinants of the velocity are the total impulse from the laser and the total areal mass of the target.

We proceeded to explore the impact of radiation on the evolution of the Be. In simulations done with xenon gas, as shown in Fig. 4, there is a distinct difference in the beryllium profile when radiation is turned off, which might or might not be due entirely to the xenon acting as a radiation source on the beryllium. To explore the relative importance of radiation from the Xe, we performed simulations identical to those described above, removing xenon gas and replacing it with helium gas at the same mass density, 0.006 g/cm^3. The He plasma produced by the shock is not a strong radiation source. Therefore, differences in the beryllium profile between cases with radiation or with radiation suppressed would be caused only by radiative effects in the Be. Shown in Fig. 5 are the results of simulations over 10 ns with beryllium driven into He gas, with multigroup radiation transport (solid line) and with radiation artificially suppressed (dashed line). The dense feature in both of these simulations is the beryllium. After 10 ns, the beryllium density profile in the radiative simulation is significantly different than in the nonradiative simulation. While the position and density of the beryllium/helium interface is approximately the same in the two simulations, more Be lagged behind the interface in the radiative case, and in this case the peak Be density is less than half the peak density in the nonradiative simulation. We conclude that the radiation treatment in the simulation has a significant effect on the beryllium behavior. However, the difference in the position of the Be/He interface is negligible between these two cases, so the effect of the radiation within the Be during the laser pulse appears not to explain the discrepancy we are exploring.

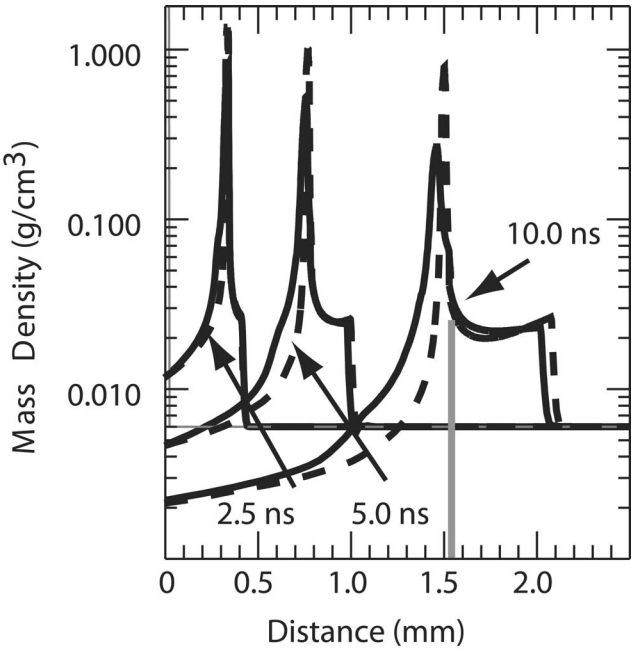

FIG. 5. Simulations of laser driven beryllium into 0.006 g/cm^3 helium gas. These simulations are identical to simulations done of the experimental setup described, except using a weakly radiating fluid. Solid lines are simulations with diffusive multigroup radiative transport, while the dashed lines are simulations with radiation artificially suppressed. Note the marked difference in the density profile of the beryllium at 10 ns between the two simulations. The vertical gray line shows the interface location at 10 ns.

The third issue we explored is the impact of the radiation

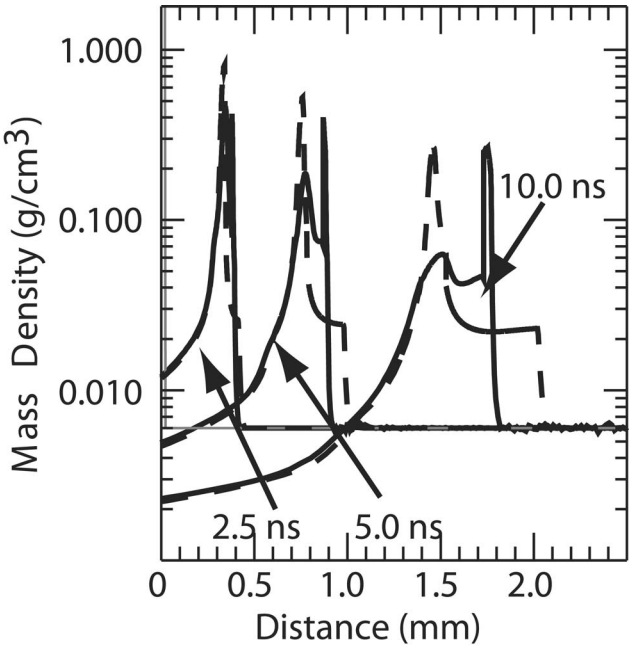

FIG. 6. Multigroup simulations of a beryllium disk driven into xenon (solid lines) and helium (dashed lines). At 2.5 ns, the difference in the beryllium structure and interface position between the two simulations is minimal. By 10 ns, the difference in the structure of the beryllium is quite different. At this time, the beryllium/xenon interface has moved 250 μm further than the beryllium/helium interface. The beryllium in the xenon simulation at this time also has significantly more material to the right of the density peak, caused by flow of beryllium ablated by the xenon radiation source.

from the xenon on the Be and on the Be/Xe interface position. In Fig. 6 we compare simulations using multigroup radiation transport in xenon gas (solid line) to those in helium gas (dashed line) at times up to 10 ns. At 2.5 ns, the difference in the beryllium profile between these two simulations is minimal. But as the radiatively collapsed layer becomes more defined, the differences become more dramatic. At 10 ns, the peak density of the beryllium driven into xenon gas is less than 1/3 that of the peak density of the beryllium driven into helium gas. The xenon simulation very clearly shows that the dense Be is ablated by the radiation. Moving from the position of the peak Be density to the Be/Xe interface, the Be both accelerates and heats in the presence of the absorption of radiative energy. Thus, this is an ablative expansion and not an adiabatic one (which also would be seen in the He simulation if present, but is not). In the simulation shown, the position of the interface in the xenon simulation is approximately 1750 μm, while that in the helium simulation is at 1500 μm, as compared to 1325 μm in the experiment. The profiles to the left of the beryllium density peaks are the same in both simulations. We discuss this case further in the next section.

V. DISCUSSION AND CONCLUSION

In the present sequence of experiments, we have established methods by which a strongly radiative shock can be driven and diagnosed in an initially planar geometry. The experiments have produced very thin shocked xenon layers, inferred to have densities several times their initial postshock values. The shocked xenon reaches temperatures of hundreds of eV near the shock front, which is why it is so strongly radiative. This type of target, and variations on it with different gases and target details, can be used in future work with increasingly advanced diagnostics, in order to achieve a detailed knowledge of the structure of radiative shocks that are optically thin upstream and optically thick downstream.

While many features in the observed data are qualitatively sensible and roughly consistent with simple models, more detailed comparisons with one-dimensional simulations revealed a disparity in the location of the Be/Xe interface. The experimental interfaces move more slowly than those in the simulations, despite the fact that the simulations are run in a way that has previously been benchmarked by purely hydrodynamic experiments. The limited two-dimensional simulations available to us did not immediately resolve these discrepancies.

This led to the scaling studies with one-dimensional simulations that have been discussed here. Potential errors in the equation of state of Be and in the radiation transport in the Be during laser irradiation do not appear able to account for the discrepancy. If the ablation of the leading edge of the Be by the radiation from the shocked Xe were weaker than predicted, this might reduce the discrepancy but would not eliminate it.

This last point merits some further discussion. It is quite plausible that errors in the opacity of the Be to the thermal radiation near 60 eV in temperature from the dense Xe layer might be incorrectly treated in the code, that there might in fact be less expansion of the Be toward the Xe, and that as a result the interface might move less far than in the standard simulation. However, it would be very difficult for this to cause the interface to end up at the observed location, moving more slowly than is reported in the nonradiative simulation with He gas. This would require that the radiation in the xenon decelerated the Be without producing much expansion from its surface. To some degree, one could explore this issue by varying the opacity of the driving material to the thermal x rays. One concludes at present that an improved treatment of radiation from the Xe layer and opacity of the Be might decrease the disparity between simulated and observed interface positions, but is unlikely to be the full explanation.

Beyond the opacity studies just mentioned, we see no other issues in the one-dimensional behavior that might explain the observed discrepancy. This suggests, for future work, a return to two-dimensional simulations and in particular a detailed examination of the lateral heat transport as a function of space and time. This potentially could reduce the ablation pressure to the level required to explain the observations.

Even after the discrepancy in interface position is resolved, it seems likely that reproducing the observed structures will prove challenging for radiation hydrodynamic codes. The dense xenon layer is optically quite thick, while the region around it is optically thin. The postshock cooling layer poses significant challenges as it is optically thin with large temperature gradients. The evaluation of the radiation

reaching the walls and their resulting expansion may also prove difficult to model.

ACKNOWLEDGMENTS

The authors wish to acknowledge the Michigan target fabrication team and the Omega technical staff, without which none of the experimental data would have been possible. We also acknowledge our long-term collaborators in these experiments at Lawrence Livermore National Laboratory, including but not limited to Bruce Remington, Gail Glendinning, and Ted Perry.

This work is supported by the National Nuclear Security Agency under DOE Grants No. DE-FG52-03NA00064, No. DE-FG52-07NA28058, and by other grants and contracts.

[1] R. P. Drake and A. B. Reighard, in *Shock Compression of Condensed Matter*, AIP Conference Proceedings, edited by M. D. Furnish, M. Elert, T. P. Russell *et al.* (AIP, Baltimore, MD, 2006), Vol. 1, pp. 1417.
[2] P. A. Keiter, R. P. Drake, T. S. Perry *et al.*, Phys. Rev. Lett. **89**, 165003 (2002).
[3] J. C. Bozier, G. Thiell, J. P. Le-Breton *et al.*, Phys. Rev. Lett. **57**, 1304 (1986).
[4] J. Grun, J. Stamper, C. Manka *et al.*, Phys. Rev. Lett. **66**, 2738 (1991).
[5] M. Busquet, High Energy Density (to be published).
[6] M. González, C. Stehlé, E. Audit *et al.*, Laser Part. Beams **24**, 535 (2006).
[7] M. Koenig, A. Benuzzi-Mounaix, N. Grandjouan *et al.*, *Shock Compression of Condensed Matter*, AIP Conference Proceedings, edited by M. D. Furnish, Y. Horie, and N. N. Thadhani (AIP, Baltimore, MD, 2001), p. 1367.
[8] S. Bouquet, C. Stéhlé, M. Koenig *et al.*, Phys. Rev. Lett. **92**, 225001 (2004).
[9] M. Koenig, T. Vinci, A. Benuzzi-Mounaix *et al.*, Astrophys. Space Sci. **298**, 69 (2005).
[10] T. Vinci, Phys. Plasmas **13**, 010702 (2006).
[11] M. Koenig, T. Vinci, A. Benuzzi-Mounaix *et al.*, Phys. Plasmas **13**, 056504 (2006).
[12] J. M. Laming and J. Grun, Phys. Rev. Lett. **89**, 125002 (2002).
[13] J. F. Hansen, M. J. Edwards, D. H. Froula *et al.*, Phys. Plasmas **13**, 022105 (2006).
[14] M. J. Edwards, A. J. MacKinnon, J. Zweiback *et al.*, Phys. Rev. Lett. **87**, 085004 (2001).
[15] R. A. Chevalier, Science **276**, 1374 (1997).
[16] J. M. Blondin, B. Fryxell, and A. Konigl, Astrophys. J. **360**, 370 (1990).
[17] A. B. Fokin, G. Massacrier, and D. Gillet, Astron. Astrophys. **420**, 1047 (2004).
[18] J. M. Blondin, E. B. Wright, K. J. Borkowski *et al.*, Astrophys. J. **500**, 342 (1998).
[19] R. P. Drake, *High-Energy-Density Physics: Foundations of Inertial Fusion and Experimental Astrophysics* (Springer, New York, 2006).
[20] L. Ensman and A. Burrows, Astrophys. J. **393**, 742 (1992).
[21] A. B. Reighard, R. P. Drake, K. K. Dannenberg *et al.*, Phys. Plasmas **13**, 082901 (2006).
[22] T. Boehly, R. S. Craxton, T. H. Hinterman *et al.*, Rev. Sci. Instrum. **66**, 508 (1995).
[23] S. Skupsky, R. W. Short, T. J. Kessler *et al.*, J. Appl. Phys. **66**, 3456 (1989).
[24] K. S. Budil, T. S. Perry, P. M. Bell *et al.*, Rev. Sci. Instrum. **67**, 485 (1996).
[25] A. B. Reighard, R. P. Drake, T. Donajkowski *et al.*, Rev. Sci. Instrum. **77**, 10E504 (2006).
[26] A. B. Reighard, R. P. Drake, K. K. Dannenberg *et al.*, in *Proceedings of Inertial Fusion Science and Applications Conference* (American Nuclear Society, Monterey, CA, 2003), Vol. 1, pp. 950.
[27] L. M. Barker and J. Hollenback, J. Appl. Phys. **43**, 1669 (1972).
[28] J. T. Larsen and S. M. Lane, J. Quant. Spectrosc. Radiat. Transf. **51**, 179 (1994).
[29] SESAME: The Los Alamos National Laboratory, Equation of State Database, LA-UR-92-3407 1992
[30] D. G. Braun, personal communication, 2000.
[31] R. P. Drake, D. R. Leibrandt, E. C. Harding *et al.*, Phys. Plasmas **11**, 2829 (2004).
[32] S. G. Glendinning, personal communication, 2006.
[33] D. R. Leibrandt, R. P. Drake, and J. M. Stone, Astrophys. Space Sci. **298**, 273 (2004).
[34] D. R. Leibrandt, R. P. Drake, A. B. Reighard *et al.* Astrophys. J. **626**, 616 (2005).